*Journal of Zhejiang University-SCIENCE A (Applied Physics & Engineering)* 2024 25(12):1006-1017
www.jzus.zju.edu.cn; www.springer.com/journal/11582
E-mail: jzus_a@zju.edu.cn

**Research Article**

https://doi.org/10.1631/jzus.A2300492



# Investigation on the resilient modulus of soil mixture at various water contents and coarse grain contents under train moving loads

Yu SU[1,2], Yue ZHANG[1], Junyi DUAN[1]✉, Jianglin GAO[2], Zhongzheng WANG[3], Da LIU[2], Bo HAN[1], Wenzhe ZHU[1]

[1]*School of Infrastructure Engineering, Nanchang University, Nanchang 330031, China*
[2]*Jiangxi Provincial Technology Innovation Center for Ecological Water Engineering in Poyang Lake Basin, Jiangxi Academy of Water Science and Engineering, Nanchang 330029, China*
[3]*School of Mechanical, Medical and Process Engineering, Faculty of Engineering, Queensland University of Technology, Brisbane QLD 4001, Australia*

**Abstract:** Interlayer soil in railway substructures is characterized by a fine/coarse soil mixture. Considering that the resilient modulus $M_r$ of the mixture is influenced by the microstructure of fine soil, it is worthwhile to investigate this aspect further. In this study, the microstructure of fines was explored by mercury intrusion porosimetry (MIP), and its influence on the $M_r$ of the mixture was studied by multi-stage dynamic triaxial tests with varying deviator stress amplitudes $\sigma_d$. The results showed a fine matrix fabric obtained at water contents of fine soil $w_f$=17.6% and 13.7% (>the plastic limit of fine soil $w_p$=12%), and a fine aggregate fabric identified at $w_f$=10.6% (<$w_p$=12%). Interestingly, the influences of $w_f$ and $\sigma_d$ on the $M_r$ of the mixture were observed: the rise in $\sigma_d$ contributed to a decline in $M_r$ when $w_f$>$w_p$ but to an increase in $M_r$ when $w_f$<$w_p$. It was concluded that, for the fine matrix fabric ($w_f$>$w_p$), increasing $\sigma_d$ induced a reduction in $M_r$, while for the fine aggregate fabric ($w_f$<$w_p$), increasing $\sigma_d$ gave rise to the growth of $M_r$. The distinct $M_r$-$\sigma_d$ behaviors for these two fabrics were explained by the competing influences between soil hardening upon loading and soil rebounding upon unloading. For the fine matrix fabric ($w_f$>$w_p$), considering its high deformability, the rebounding effect on $M_r$ outweighed the hardening effect, and thus a decline in $M_r$ occurred with the growth of $\sigma_d$. Conversely, for the fine aggregate fabric ($w_f$<$w_p$), the rebounding effect on $M_r$ was secondary compared with the hardening effect based on the consideration of its low deformability, and thus an increase in $M_r$ was observed with rising $\sigma_d$.

**Key words:** Railway engineering; Resilient modulus; Unsaturated soil; Microstructure

## 1 Introduction

An interlayer in the railway substructure commonly forms owing to decades of train moving loads. In-situ observation shows that this interlayer soil consists of ballast grains and subgrade fines. With an increasing depth of the interlayer, the ballast grain content declines (Trinh, 2011). As a component of the railway substructure, the resilient modulus $M_r$ of interlayer soil is a crucial parameter for the performance of rail tracks. With the ongoing demand for increased axle loads in railway transportation, the deviator stress amplitudes $\sigma_d$ (determined by the subtraction between the maximum and the minimum deviator stresses for one loading cycle) increase, which facilitates the degradation of the ballast and thus causes a reduction in its resilient modulus (Indraratna et al., 2021). On the other hand, the water level in the field varies frequently, which facilitates the variation in $M_r$ of the soil mixture. To obtain a thorough understanding of $M_r$ of the soil mixture, it is necessary to explore this parameter at distinct water contents and coarse grain contents under train moving loads.

The impact of water content on the $M_r$ of railway subgrade soil was examined: under saturation, an accumulation of pore water pressure was induced by traffic loadings, which resulted in a decline in $M_r$. With a reduction in the water content, $M_r$ increased because of the suction effect (Duong et al., 2013; Ng et al., 2019; Wang et al., 2019; Wan et al., 2020; Zheng et al., 2020; Hu and Bian, 2022; Bian et al., 2023). Lokkas et al. (2021) suggested that soil behavior is crucial for the

✉ Junyi DUAN, jyduan91@ncu.edu.cn
Junyi DUAN, https://orcid.org/0000-0002-1798-833X

Received Oct. 3, 2023; Revision accepted Dec. 26, 2023;
Crosschecked Mar. 15, 2024; Online first Apr. 15, 2024

infrastructure. Alamanis et al. (2021) developed the assessment principles for the shear strength of clayey soil by experiments. Anagnostopoulos et al. (2020) explored the shear strength parameters of grouted coarse soil, and found that the injectability of cement grouts into coarse soil contributed to an increase in its cohesion. Sun et al. (2018) performed dynamic triaxial tests on railway ballast and reported that a large reduction of $M_r$ occurred with an increasing coefficient of uniformity. Wang et al. (2017) carried out dynamic triaxial tests to address the influence of coarse grain content $f_v$ on the $M_r$ of the soil mixture. They identified a characteristic value $f_{v-cha}$; with an increase in $f_v$, a slow rising rate of $M_r$ was observed when $f_v<f_{v-cha}$ while a fast rising rate of $M_r$ occurred when $f_v>f_{v-cha}$. This was because the former was characterized by a fine soil-supported fabric, while the latter featured a coarse grain-supported fabric. Duong et al. (2016) addressed the influences of water content $w$ and $f_v$ on the $M_r$ of the soil mixture. They reported that the growth of $f_v$ facilitated the increase in $M_r$ at saturation but a decline in $M_r$ at unsaturation. It should be noted that in previous studies, a stable dry density of soil mixture $\rho_d$ was controlled for the mixture with different $f_v$ values. Under this circumstance, the dry density of fine soil fraction $\rho_{d-f}$ declined with an increase in $f_v$, which induced a reduction in suction. As a result, both $f_v$ and suction changed, rendering the test results difficult to analyze.

Lekarp et al. (2000) reviewed the influence of various factors (e.g., confining pressure ($\sigma_3$) and $\sigma_d$) on the $M_r$ of unbound aggregates and found that $\sigma_3$ and $\sigma_d$ played important roles. Sun et al. (2016) executed dynamic triaxial tests to address the effects of $\sigma_3$ and $\sigma_d$ on the $M_r$ of ballast and found that it rose with increasing $\sigma_3$ and $\sigma_d$. Ng et al. (2013) worked on the effect of $\sigma_d$ on the $M_r$ of subgrade soil, and indicated that an increase in $\sigma_d$ induced a decline in $M_r$ at a low suction $\psi$ ranging from 0 to 250 kPa (the corresponding $w$ ranged from 20.5% to 6.8%). Yang et al. (2008) explored the $M_r$ of cohesive soil with various $\sigma_d$ and $\psi$ values: with the growth of $\sigma_d$, the $M_r$ declined at low $\psi$=50 and 150 kPa ($w$=23.2% and 20.2%) but increased at high $\psi$=450 kPa ($w$=19.1%). Su et al. (2021b) executed dynamic triaxial tests to address the combined influences of $\sigma_d$ and $w$ on the $M_r$ of mixture. In their study, an increase in $\sigma_d$ induced a decline in $M_r$ at high $w$=17.6% but an increase in $M_r$ at low $w$=10.6%. However, these studies focused solely on the influences of traffic loading and $w$ (or $\psi$) on the $M_r$ of soil and failed to explore its microstructural mechanism, especially of the soil mixture. Notably, in this study, the $M_r$ of soil was obtained by performing dynamic triaxial tests and microstructure observation was conducted by mercury intrusion porosimetry (MIP). Based on the results, it is vital to explore the relationship between the $M_r$ of the soil mixture and its microstructure.

The purpose of the present research was to identify the impacts of $w$, $f_v$, and $\sigma_d$ on the $M_r$ of the soil mixture in the conventional railway substructure. Multistage dynamic triaxial tests were executed, allowing the determination of $M_r$ under varying $w$, $f_v$, and $\sigma_d$ values. MIP was carried out to examine the influence of water contents of fine soil $w_f$ on the microstructure of fine soil fraction. The results allowed us to shed light on the relationship between the variation in $M_r$ and that in the microstructure.

## 2 Materials and methods

### 2.1 Reconstituted fine soil and micro-ballast

In our laboratory experiment, the intact interlayer soil was substituted by a mixture of reconstituted fines and micro-ballast. Fig. 1a compares the grain size distribution (GSD) curves of reconstituted fine soil and natural fine soil, which show good agreement. Note that the reconstituted fines consist of a small proportion of clay content (30%) and a large proportion of sand content (70%) (Wang et al., 2017). The soil properties of reconstituted fines were as follows: the optimum water content $w_{opt-f}$=13.7% and the maximum dry density $\rho_{dmax-f}$=1.82 Mg/m$^3$. Fig. 1b presents the GSD curves of ballast and micro-ballast (more details in (Qi et al., 2020b)). In accordance with Qi et al. (2020a), the parameter of $f_v$ was employed to describe the number of micro-ballast in the mixture (more details can be seen in Section S1 of the electronic supplementary materials (ESM)). The cohesion $c$ and friction angle $\varphi$ of fine/coarse soil mixture with varying $f_v$ values were presented in Table 1, which were obtained from Su et al. (2020).

In this study, a constant $\rho_{d-f}$ value (1.82 Mg/m$^3$), three target $w_f$ values (17.6%, 13.7%, and 10.6%), and five target $f_v$ values (0%, 10%, 20%, 35%, and 45%) were considered. Table 1 presents the detailed soil properties of the samples. For the experiment, fine soil was prepared at $w_{opt-f}$=13.7%, followed by storage in a

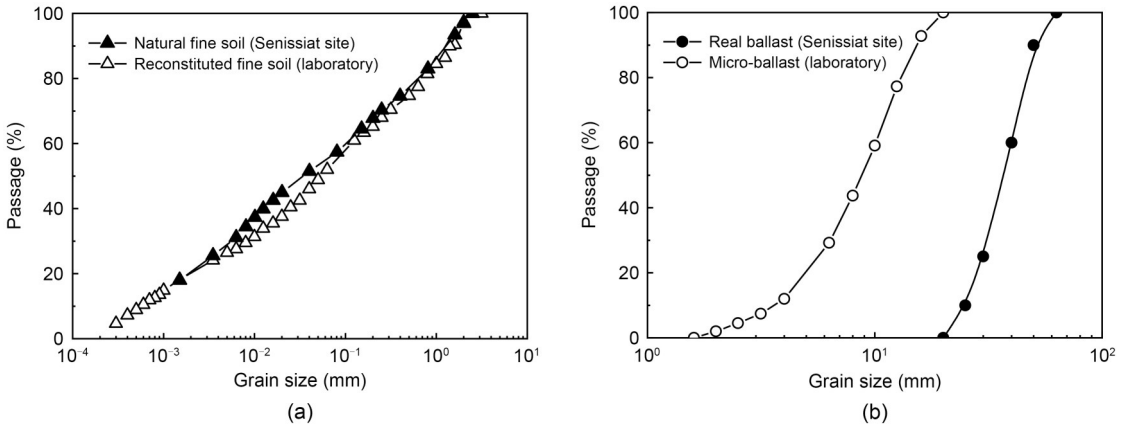


**Fig. 1 Comparisons of GSD curves for: (a) natural fine soil and reconstituted fine soil; (b) real ballast and micro-ballast**

**Table 1 Soil properties of samples in cyclic triaxial tests**

| $f_v$ (%) | Fine soil fraction | | | Soil mixture | | | Shear strength parameter | |
|---|---|---|---|---|---|---|---|---|
| | $w_{opt-f}$ (%) | Target $w_f$ (%) | Target $\rho_{dmax-f}$ (Mg/m$^3$) | Target $S_r$ (%) | Target $\rho_d$ (Mg/m$^3$) | Measured $\rho_d$ (Mg/m$^3$) | $c$ (kPa) | $\varphi$ (°) |
| 0 | 13.7 | 17.6 | 1.82 | 100 | 1.82 | 1.80 | 32 | 8 |
| | 13.7 | 13.7 | 1.82 | 78 | 1.82 | 1.82 | 61 | 15 |
| | 13.7 | 10.6 | 1.82 | 60 | 1.82 | 1.85 | 137 | 21 |
| 10 | 13.7 | 17.6 | 1.82 | 100 | 1.91 | 1.88 | 32 | 9 |
| | 13.7 | 13.7 | 1.82 | 78 | 1.91 | 1.91 | 56 | 18 |
| | 13.7 | 10.6 | 1.82 | 60 | 1.91 | 1.93 | 129 | 27 |
| 20 | 13.7 | 17.6 | 1.82 | 100 | 1.99 | 1.97 | 29 | 12 |
| | 13.7 | 13.7 | 1.82 | 78 | 1.99 | 1.99 | 52 | 21 |
| | 13.7 | 10.6 | 1.82 | 60 | 1.99 | 2.01 | 125 | 27 |
| 35 | 13.7 | 17.6 | 1.82 | 100 | 2.12 | 2.11 | 27 | 22 |
| | 13.7 | 13.7 | 1.82 | 78 | 2.12 | 2.12 | 43 | 31 |
| | 13.7 | 10.6 | 1.82 | 60 | 2.12 | 2.13 | 102 | 38 |
| 45 | 13.7 | 17.6 | 1.82 | 100 | 2.21 | 2.20 | 26 | 34 |
| | 13.7 | 13.7 | 1.82 | 78 | 2.21 | 2.21 | 30 | 38 |
| | 13.7 | 10.6 | 1.82 | 60 | 2.21 | 2.22 | 98 | 46 |

$S_r$ represents the degree of saturation of soil mixture

sealed container with a duration of at least 24 h. A soil mixture with a target $f_v$ value was obtained by mixing fine soil with coarse grains (Fig. 2a). This mixture was dynamically compacted to a cylindrical sample (Fig. 2b). Note that the $\rho_{d-f}$=1.82 Mg/m$^3$ of the fine soil was controlled to be the same for mixtures with varying $f_v$. With an increase in $f_v$, the dry density of mixture $\rho_d$ also elevated.

The as-compacted sample at $w_{opt-f}$=13.7% was then wetted or dried to the target $w_f$: $w_{1-f}$=17.6% on the wet side and $w_{2-f}$=10.6% on the dry side. To attain this purpose, the approach developed by Su et al. (2021a) was adopted: 1 h of air drying followed by an equilibration time of at least 7 h to lower the water content; conversely, 10 g water was sprayed on the sample followed by the same equilibration time to raise the water content. The wetting/drying procedures ended when the mass of sample increased to that corresponding to $w_{1-f}$=17.6% or decreased to that corresponding to $w_{2-f}$=10.6%. The wetting/drying procedures led to a slight swelling/shrinkage of the sample. Accordingly, the measured $\rho_d$ value of the sample slightly decreased or increased (Table 1).

## 2.2 Dynamic triaxial tests

The dynamic triaxial testing system adopted from Wang et al. (2017) was employed to explore the influences of $w_f$, $f_v$, and $\sigma_d$ on the $M_r$ of the soil mixture.

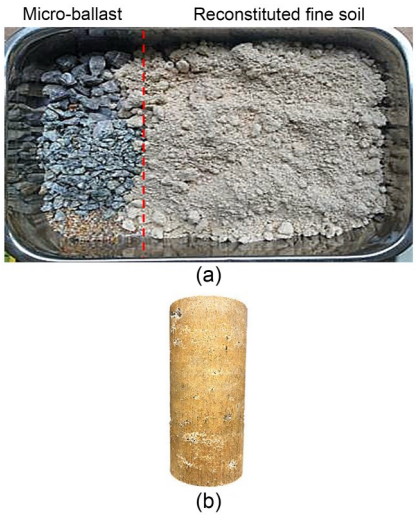


**Fig. 2 Overview of: (a) reconstituted fine soil and micro-ballast; (b) as-compacted sample**

The as-compacted cylindrical specimens (diameter $d$=100 mm and height $h$=200 mm) with three target $w_f$ values (17.6%, 13.7%, and 10.6%) and five $f_v$ values (0%, 10%, 20%, 35%, and 45%) were tested. A 50 kN hydraulic actuator was mounted, allowing for the application of repeated loading with varying shapes, amplitudes, and high-loading cycles. The axial deformation was recorded with a precision of ±0.1 mm. The force sensor at the bottom allows for the precise determination and refined control of the axial force, eliminating the friction between the loading piston and the testing chamber.

A value of $\sigma_3$=30 kPa was set, which was equivalent to in-situ horizontal stress based on the consideration of the depth of interlayer soil and the train moving load (Trinh et al., 2012). For $w_{1-f}$=17.6% ($S_r$=100%), $\sigma_3$=30 kPa was employed, followed by overnight consolidation to allow for the dissipation of generated pore water pressure. Afterwards, the specimen was sheared. For $w_{opt-f}$=13.7% ($S_r$=78%) and $w_{2-f}$=10.6% ($S_r$=60%), the same consolidation time of one night was adopted under $\sigma_3$=30 kPa before shearing. All testing procedures were executed in accordance with ASTM D7181-11 (ASTM, 2011). Fig. 3a shows an increase in $\sigma_d$ from 10 to 30 kPa in the loading procedure. These $\sigma_d$ values ranging from 10 to 30 kPa were selected based on considering axial stress in varying depths of interlayer soil from 250 to 600 mm, which were consistent with Wang et al. (2018b). A number of repeated loading cycles, $N$=90000, was employed for a given $\sigma_d$, which was considered to be large enough for the stabilization of

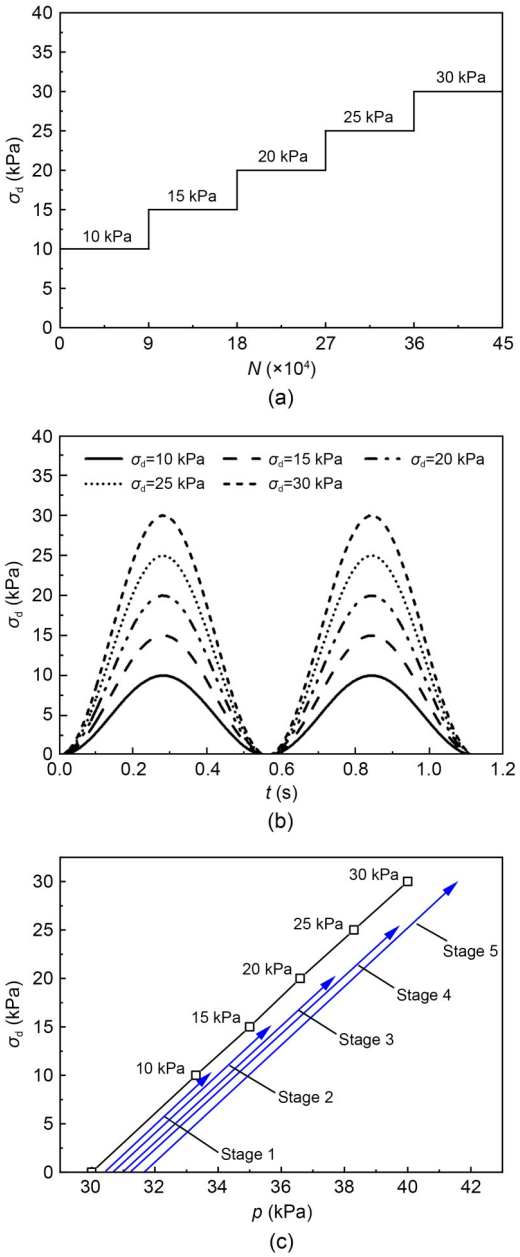


**Fig. 3 (a) Multi-stage loading procedure; (b) sine-shaped signals; (c) stress path for varying $\sigma_d$**

a resilient modulus (Gidel et al., 2001; Lamas-López, 2016; Qi et al., 2020b). A loading frequency of 1.78 Hz was set (Fig. 3b), equal to that generated under a train speed of 50 km/h in conventional rail tracks. Fig. 3c presents a constant stress ratio $\sigma_d/\Delta p$=3 for varying $\sigma_d$ values, which was a typical in-situ stress path ($p$ represents the mean principal stress, and $\Delta p$ is the increment of the mean principal stress). In these tests, the evolution of deviator stress and axial deformation with time was measured.

### 2.3 MIP tests

In this study, MIP tests were conducted, which allowed for observing the microstructure of fines with different $w_f$ values. Three samples at a constant $f_v$=0% and varying $w_f$=17.6%, 13.7%, and 10.6% were prepared, respectively. The freeze-drying method used by Zhang et al. (2018) was implemented to prepare the fine soil for the MIP test: a piece of fine soil (around 1.5 g) was put into liquid nitrogen under vacuum, followed by storage for at least 24 h in the freeze dryer chamber for sublimation. This method can minimize the microstructure disturbance during dehydration to a large extent, ensuring the quality of MIP results (Delage et al., 2006; Zhang et al., 2018). An Autopore IV 9500 porosimeter (Micromeritics Instrument Corporation, USA) was used, allowing the measurement of pore diameter ($D$) in the 0.006–350.000 μm range.

## 3 Experimental results

### 3.1 Variations in resilient modulus with $w_f$, $f_v$, and $\sigma_d$

Fig. 4 shows the evolution of hysteresis loops with $N$ from 0 to 90000 for the samples at $f_v$=0%, $w_{1-f}$=17.6%, and $\sigma_d$=10 kPa. Under a given hysteresis loop, the axial strain $\varepsilon_1$ consists of permanent strain $\varepsilon_1^p$ and resilient strain $\varepsilon_1^r$. The resilient modulus $M_r$ was determined by the ratio of $\sigma_d$ to $\varepsilon_1^r$ in one cycle, which is also the secant slope of the hysteresis loop (for the resilient strain part in Fig. 4). With the progression of $N$, the size of the hysteresis loop reduced. When the end of the loading stage was reached (e.g., $N$>10000), the hysteresis loop became stable. This can be explained as follows: at the beginning of the loading cycles, the reorientation and rearrangement of particles produced a larger plastic strain $\varepsilon_1^p$. As $N$ increased, more inter-particle contacts developed, initially inducing a smaller plastic strain and finally a purely resilient state. Similar observations were made by Werkmeister et al. (2001, 2004).

Fig. 5a shows the evolutions of the end-stage (at $N$=90000 for each loading stage) hysteresis loops with

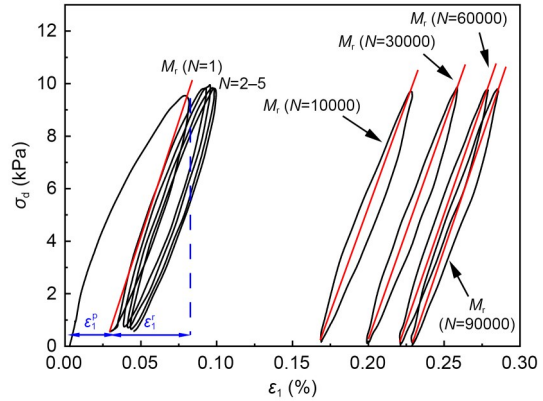


**Fig. 4 Plots of typical hysteresis loops for the sample of $f_v$=0%, $w_{1-f}$=17.6%, and $\sigma_d$=10 kPa**

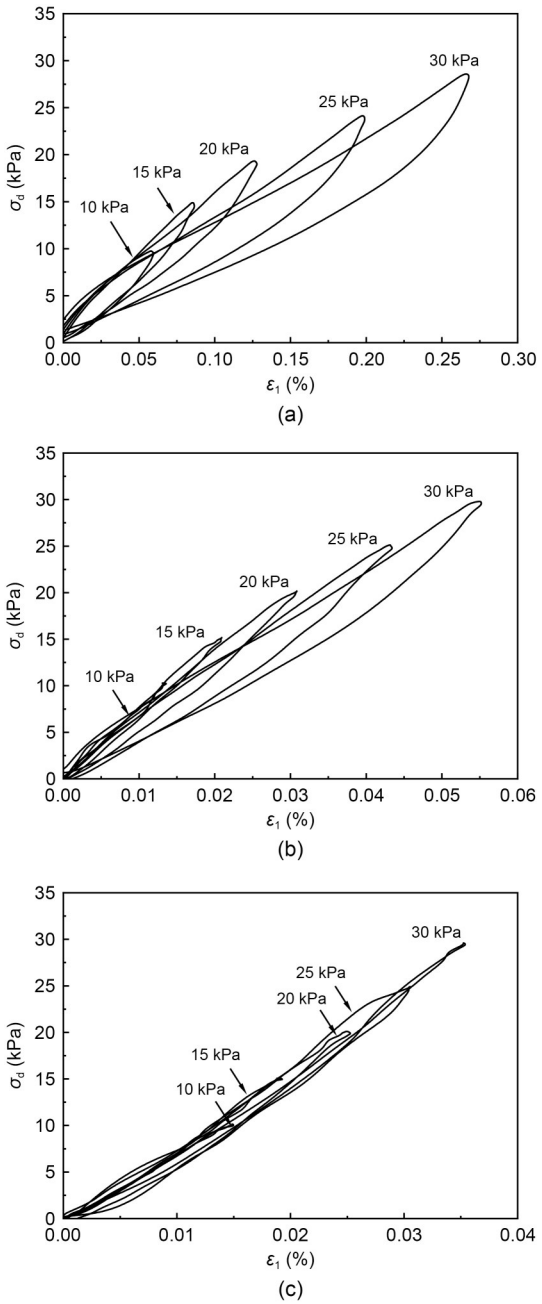


**Fig. 5 Plots of end-stage hysteresis loops versus $\sigma_d$ for: (a) $w_{1-f}$=17.6%; (b) $w_{opt-f}$=13.7%; (c) $w_{2-f}$=10.6%**

$\sigma_d$ under $f_v$=0% for $w_{1-f}$=17.6%. An increment of $\sigma_d$ induced an increasing size of the hysteresis loop. Meanwhile, the secant slope of the hysteresis loop decreased as $\sigma_d$ increased, suggesting that the corresponding $M_r$ decreased. A similar observation was identified for the sample of $f_v$=0% and $w_{opt-f}$=13.7%, as shown in Fig. 5b. By contrast, for the sample of $f_v$=0% and $w_{2-f}$=10.6% in Fig. 5c, increasing $\sigma_d$ induced the slight growth of the secant slope and thus a slight increment of $M_r$ accordingly. The decrease of $w_f$ from $w_{1-f}$=17.6% (Fig. 5a) to $w_{2-f}$=10.6% (Fig. 5c) induced a decline of axial strain $\varepsilon_1$ due to the suction effect, which contributed to an increase of $M_r$.

Fig. 6a shows variations of $\varepsilon_1^r$ with $N$ under $f_v$=0% for $w_{1-f}$=17.6%. At a constant $\sigma_d$, the $\varepsilon_1^r$ increased rapidly during the early loading cycles, followed by a gradually decreasing trend until reaching stabilization. This was because the cyclic loading led to a denser structure with increasing $N$, and thus a decrease of $\varepsilon_1^r$. When more contacts of particles were developed, the $\varepsilon_1^r$ became stable, as shown by Duong et al. (2016). With an increase of $\sigma_d$, the $\varepsilon_1^r$ increased. Similar observations were identified for the samples with $w_{opt-f}$=13.7% in Fig. 6b and $w_{2-f}$=10.6% in Fig. 6c.

Figs. 7a–7c present evolutions of $M_r$ with $N$ under varying $f_v$ and $\sigma_d$ values for $w_f$=17.6%, 13.7%, and 10.6%, respectively. In Fig. 7a ($w_{1-f}$=17.6%), under a constant $\sigma_d$, $M_r$ increased slightly with the increasing $N$, which was attributed to the slight decrease of $\varepsilon_1^r$ with $N$ in Fig. 6a. Note that as stated by Werkmeister et al. (2004), under the effect of cyclic loading, the particle rotation and rearrangement occurred. This contributed to a denser structure of soil mixture and thus an increase of its $M_r$ value. The similar observation was made by Duong et al. (2016) on soil mixture with varying $f_v$= 50% and 56%, who found that the $M_r$ of mixture increased with increasing loading cycle. An increment of $\sigma_d$ induced a decline of $M_r$. In addition, increasing $f_v$ led to an increase of $M_r$ slightly at $f_v$=0%–20%, while significantly at $f_v$=35%–45%. This was attributed to the change of soil fabric: a fine soil supported fabric at $f_v$= 0%–20% and a coarse grain supported fabric at $f_v$= 35%–45%, as evidenced by Wang et al. (2018b). Similar observation was made for the samples with $w_{opt-f}$= 13.7% in Fig. 7b. Conversely, for the sample with $f_v$= 0% and $w_{2-f}$=10.6% in Fig. 7c, increasing $\sigma_d$ contributed to an increment of $M_r$. Note that for the case of $w_{2-f}$= 10.6%, only the $M_r$ at $f_v$=0% was presented. That was

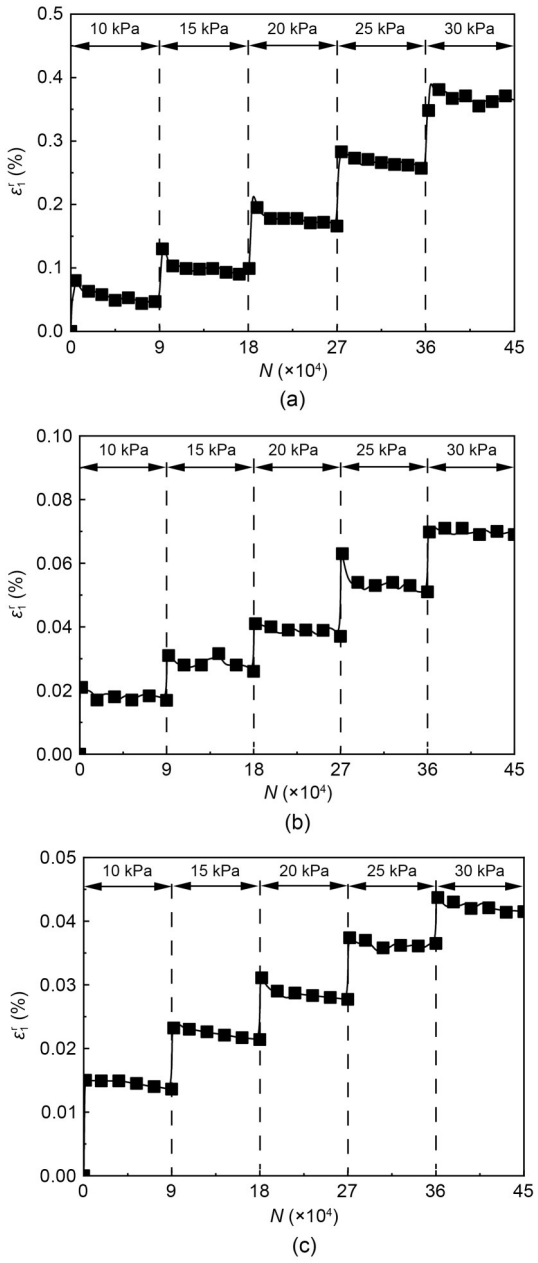


**Fig. 6 Plots of $\varepsilon_1^r$ versus $N$ for: (a) $w_{1-f}$=17.6%; (b) $w_{opt-f}$= 13.7%; (c) $w_{2-f}$=10.6%**

because the axial strain $\varepsilon_1$ at $f_v$=10%–45% was beyond the capacity (±0.1 mm) of the axial strain using the testing system. Consequently, the determination of $M_r$ for the samples with $w_{2-f}$=10.6% and $f_v$=10%–45% was not accurate due to the testing limitation, and thus is not depicted in Fig. 7c.

### 3.2 Variations of pore size distributions with $w_f$

Fig. 8 presents the pore size distributions (PSDs) of the fine soil for the samples at $f_v$=0% and $w_f$=17.6%,

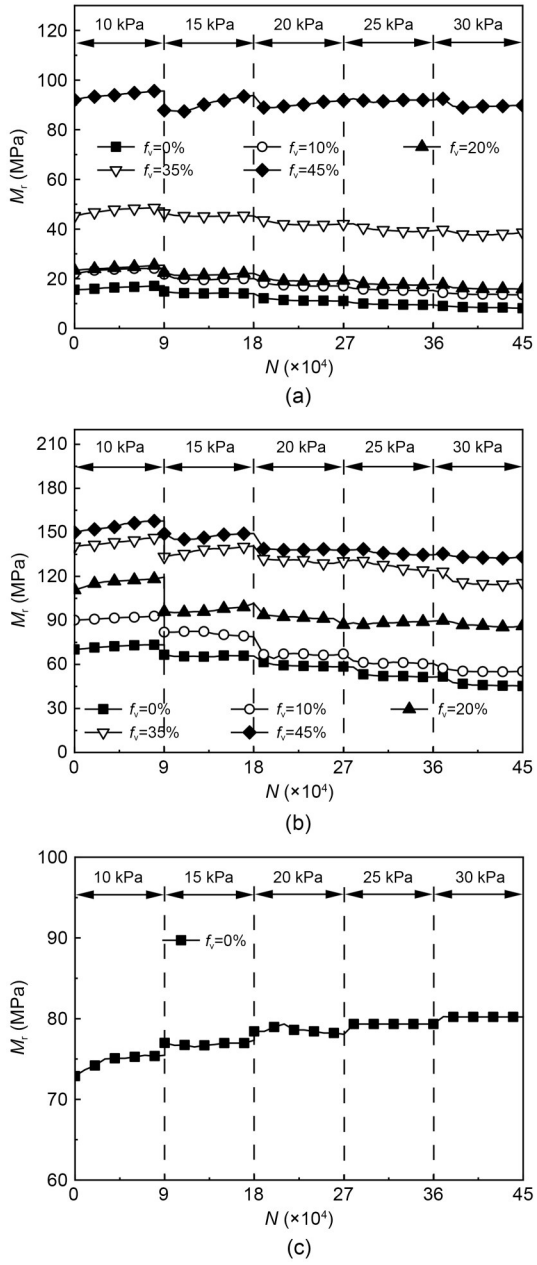


**Fig. 7 Plots of $M_r$ versus $N$ for: (a) $w_{1\text{-f}}$=17.6%; (b) $w_{\text{opt-f}}$=13.7%; (c) $w_{2\text{-f}}$=10.6%**

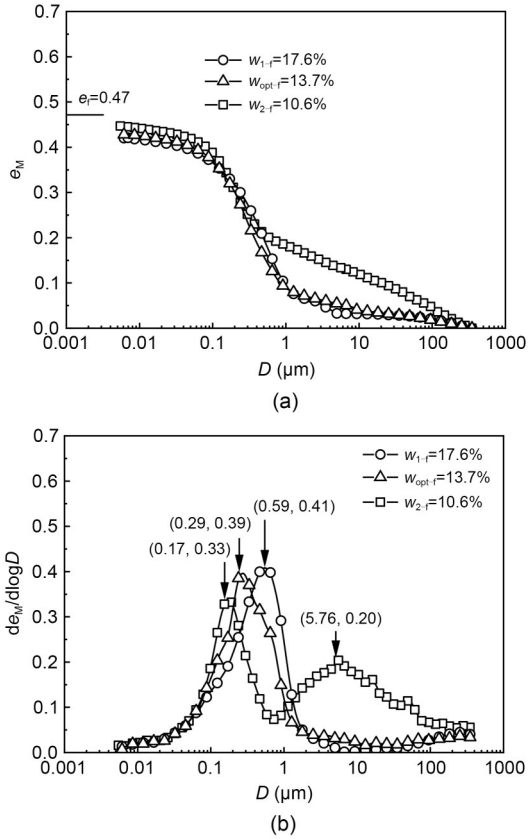


**Fig. 8 PSDs of fine soil at $f_v$=0% and varying water contents: (a) cumulative curves; (b) density function curves**

13.7%, and 10.6%. Note that, as depicted by Muñoz-Castelblanco et al. (2012), the mercury intruded void ratio of fine soil $e_M$ was determined by the ratio between the volume of intruded mercury $V_{Hg}$ and that of the solid phase $V_s$. The $V_{Hg}$ was directly obtained from MIP tests, while the $V_s$ is the ratio between the mass of solid $m_s$ and the density of solid $\rho_s$ ($\rho_s$=2.67 Mg/m$^3$ in (Duong et al., 2013)). In Fig. 8a, the $e_M$ was slightly smaller than the void ratio of fine soil $e_f$=0.47. In Fig. 8b, a unimodal porosity structure was observed for the samples at $w_{1\text{-f}}$=17.6% and $w_{\text{opt-f}}$=13.7%, with only a micro-pore population identified. However, a bimodal porosity structure was obtained for the sample with $w_{2\text{-f}}$=10.6%, with both micro-pore and macro-pore populations characterized. This can be explained below: on the wet side of optimum ($w_{1\text{-f}}$=17.6%) and at the optimum ($w_{\text{opt-f}}$=13.7%), a fine matrix fabric was formed due to water hydration, leading to a unimodal microstructure. As the water content declined, aggregation of the fine soil occurred, as evidenced by Cui and Delage (1996). A fine aggregate fabric was obtained on the dry side of optimum ($w_{2\text{-f}}$=10.6%), resulting in a bimodal microstructure. The similar phenomenon was reported by Delage et al. (1996). An increment of $w_f$ from $w_{2\text{-f}}$=10.6% to $w_{\text{opt-f}}$=13.7% and $w_{1\text{-f}}$=17.6% contributed to the growth of the size of the main micro-pores from 0.17 to 0.29 and 0.59 μm, respectively. This was explained by that increasing $w_f$ induced the swelling of fine soil due to the aforementioned clay fraction (around 30.0%) contained in fine soil (Fig. 1), and thus causing an increase of $D$. This was in accordance with the observations of Li and Zhang (2009).

## 4 Interpretation and discussion

### 4.1 Combined effects of $w_f$ and $\sigma_d$ on $M_r$

Fig. 9 shows evolutions of the end-stage $M_r$ with $w_f$ under varying $\sigma_d$=10–30 kPa for $f_v$=0%. A threshold water content $w_{th}$=11.3% was identified. When the $w_f$ was higher than that value, an increment of $\sigma_d$ induced a reduction of $M_r$, while a reverse trend was obtained when the $w_f$ was lower. Similar observations were reported by Wang et al. (2017) and Su et al. (2021b) on the same soil mixture with varying $f_v$=0%–45% under $\sigma_d$=50–200 kPa. The $w_{th}$=12.6%, 11.9%, 11.7%, 12.3%, and 13.0% were obtained for $f_v$=0%, 10%, 20%, 35%, and 45%, respectively (more details can be seen in Section S2 of the ESM). These values of $w_{th}$ in the present studies, Wang et al. (2017) and Su et al. (2021b), were found to be close to the plastic limit of the fine soil $w_p$=12%. It could thus be inferred that $w_p$ corresponded to the $w_{th}$ of the fine/coarse soil mixture. Interestingly, it was found from Figs. 8a and 8b that $w_p$ separated the two fabrics of fine soil: a fine matrix fabric at $w_{1-f}$=17.6% and $w_{opt-f}$=13.7% (>$w_p$=12%) and a fine aggregate fabric at $w_{2-f}$=10.6% (<$w_p$=12%). The similar observation was made by Ahmed et al. (1974) on clay and Delage et al. (1996) on silt, who found that $w_p$ was the threshold water content for a fine matrix microstructure and a fine aggregate microstructure. It can be thus inferred that for the fine matrix fabric ($w_f$>$w_p$), an increment of $\sigma_d$ induced a decline of $M_r$, while for the fine aggregate fabric ($w_f$<$w_p$), an increment of $\sigma_d$ contributed to an increase of $M_r$.

The $M_r$-$\sigma_d$ relationship for these two fabrics was the competing result between soil hardening upon loading and soil rebounding upon unloading. When loading, the growth of $\sigma_d$ facilitated the compression of fine soil, resulting in an increment of $M_r$ for both fabrics. Conversely, when unloading, the rebounding effect of fine soil led to an increment of $\varepsilon_1^r$, and thus a reduction of $M_r$. For the fine matrix fabric ($w_f$>$w_p$), with respect to its high deformability, the rebounding influence on $M_r$ outweighed the hardening influence. For instance, in Fig. 6a ($w_{1-f}$=17.6%, the fine matrix fabric), an increase of $\sigma_d$ from 10 to 15 kPa (increase by 50%) led to a large increase of end-stage $\varepsilon_1^r$ from 0.050% to 0.100% (increase by 100%). Consequently, an increment of $\sigma_d$ induced a reduction of $M_r$ for the fine matrix fabric. Conversely, for the fine aggregate fabric ($w_f$<$w_p$), the rebounding effect on $M_r$ was secondary compared with the hardening effect based on the consideration of its low deformability. As shown in Fig. 6c ($w_{2-f}$=10.6%), an increase of $\sigma_d$ from 10 to 15 kPa (increase by 50%) induced a small increase of $\varepsilon_1^r$ from 0.014% to 0.020% (increase by 42%). Thus, $M_r$ increased with increasing $\sigma_d$ for the fine aggregate fabric.

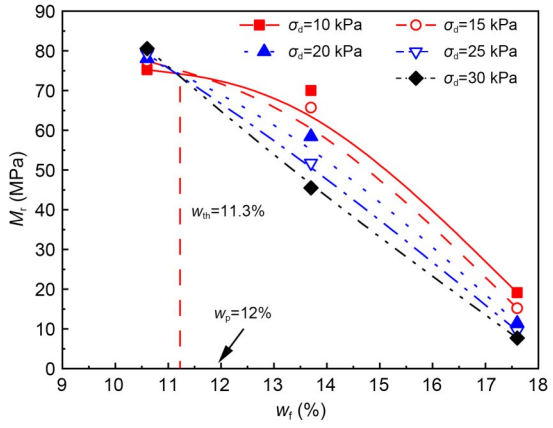


**Fig. 9 Plots of end-stage $M_r$ versus water content of fine soil $w_f$ for $f_v$=0%**

### 4.2 Combined effects of $w_f$ and $f_v$ on $M_r$

Figs. 10a and 10b show that under a given $f_v$, with increasing $\sigma_d$, the decreasing rate of $M_r$ at $w_{opt-f}$=13.7% was larger than that at $w_{1-f}$=17.6%. This phenomenon can be explained as follows: according to the findings of Ng et al. (2017), the decrease of $w_f$ from $w_{1-f}$=17.6% to $w_{opt-f}$=13.7% induced the shrinkage of soil and a decrease of void ratio (as evidenced by an increase of measured $\rho_d$ in Table 1), which gave rise to an increase of particles contacts. As stated by Werkmeister et al. (2004), the resilient deformation was referred to deformation at particle contacts. In this case, a larger increasing rate of resilient strain $\varepsilon_1^r$ was expected at $w_{opt-f}$=13.7%, and thus a larger decreasing rate of $M_r$ was obtained.

Figs. 10a and 10b show evolutions of end-stage $M_r$ with $\sigma_d$ under varying $f_v$ for $w_{1-f}$=17.6% and $w_{opt-f}$=13.7% respectively. It was found that the growth of $f_v$ induced an increment of $M_r$ under both saturation ($w_{1-f}$=17.6%) and unsaturation ($w_{opt-f}$=13.7%). A comparative work between the present study and Duong et al. (2016) was fulfilled. Duong et al. (2016) explored the $M_r$ of the soil mixture with varying $f_v$=50.3% and 55.5% for $w$=12%, 6%, and 4% (Figs. 11a–11c). They found that the growth of $f_v$ contributed to an increase of $M_r$ at saturation ($w$=12%), but a decrease of $M_r$ at unsaturation

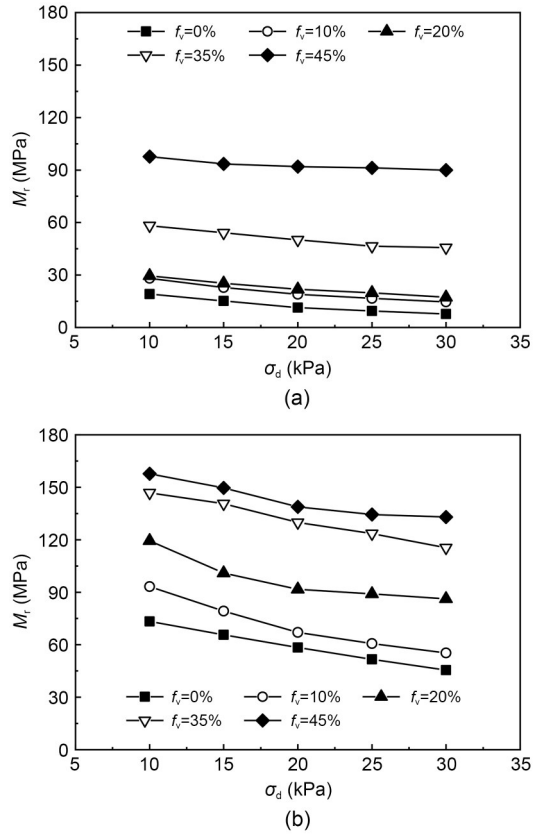


**Fig. 10 Plots of end-stage $M_r$ versus $\sigma_d$ for: (a) $w_{1-f}$=17.6%; (b) $w_{opt-f}$=13.7%**

($w$=6% and 4%). The former case ($w$=12%) is in accordance with the observation in present study (Fig. 10a), while the latter cases ($w$=6% and 4%) are opposed to that observed in present study (Fig. 10b).

The combined effects of $w_f$ and $f_v$ on $M_r$ of mixture were linked with the effect of suction $\psi$. For this study, a constant $\rho_{d-f}$=1.82 Mg/m$^3$ of fine soil was kept for varying $f_v$ (Table 1), which led to a constant $\psi$ for a given $w$ (e.g. $\psi$=739 kPa for a constant $w_{opt-f}$=13.7% and various $f_v$ values in (Wang et al., 2018a, 2018b)). This was experimentally examined by Su et al. (2022), who found that the water retention capacity of soil mixture became higher with an increment of $\rho_{d-f}$, while remained unchanged with an increment of $f_v$ when the $\rho_{d-f}$ was constant. In this case, the growth of $f_v$ induced an increment of $M_r$ under both saturation and unsaturation (Figs. 10a and 10b), which was only due to the reinforcement influence of coarse grains, while being independent of the effect of suction. Conversely, for Duong et al. (2016), given that the $\rho_d$=2.01 Mg/m$^3$ of mixture was unchanged, the growth of $f_v$ from 50.3% to 55.5% induced a reduction of $\rho_{d-f}$ from 1.33 to 1.17 Mg/m$^3$

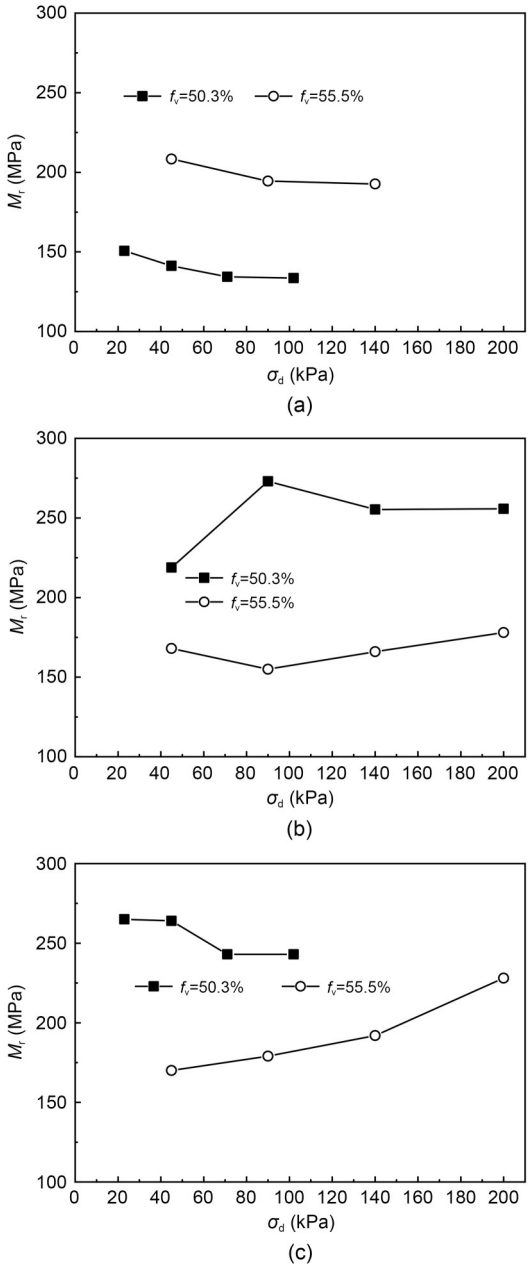


**Fig. 11 Plots of end-stage $M_r$ versus $\sigma_d$ for: (a) $w$=12%; (b) $w$=6%; (c) $w$=4%. Reprinted from (Duong et al., 2016), Copyright 2015, with permission from Springer Nature**

(Table 2), and thus a decline of $\psi$ consequently. This was evidenced by Duong et al. (2014), who reported that the growth of $f_v$ from 50.3% to 55.5% induced a decrease of water retention capacity. At saturation ($w$=12%, corresponding to $S_r$=100%, Fig. 11a), the growth of $f_v$ gave rise to an increment of $M_r$, which was explained by the only reinforcement effect of coarse grains. By contrast, at unsaturation ($w$=6% and 4%, corresponding to $S_r$=49% and 32%, respectively, Figs. 11b

and 11c), an increment of $f_v$ contributed to a decline of $\psi$. While the reinforcement effect of incrementing $f_v$ was less significant than the negative effect of declining $\psi$, the $M_r$ decreased.

**Table 2 Soil properties of Duong et al. (2016)**

| $f_v$ (%) | $w$ (%) | $S_r$ (%) | $\rho_d$ (Mg/m$^3$) | $\rho_{d-f}$ (Mg/m$^3$) |
|---|---|---|---|---|
| 50.3 | 4 | 32 | 2.01 | 1.33 |
| | 6 | 49 | 2.01 | 1.33 |
| | 12 | 100 | 2.01 | 1.33 |
| 55.5 | 4 | 32 | 2.01 | 1.17 |
| | 6 | 49 | 2.01 | 1.17 |
| | 12 | 100 | 2.01 | 1.17 |

## 5 Practical implications of present study

From a practical point of view, with increasing train moving loads, the $M_r$ of the interlayer soil increases at low water content (smaller than the $w_p$) but decreases at high water content (larger than the $w_p$). This suggests that a drainage system in the railway substructure is required, for ensuring the normal performance of interlayer soil, especially under varying train moving loads. Otherwise, a decrease in the stiffness of interlayer soil is expected.

## 6 Conclusions

This study is to address the relationship between the $M_r$ of soil mixture and the microstructure of fines. MIP tests were fulfilled for observing the fabric of fine soil at different $w_f$, while dynamic triaxial tests with varying $\sigma_d$ were carried out for the determination of $M_r$ of soil mixture with various $w_f$ and $f_v$. From these tests, the following conclusions were obtained.

(1) For the fine matrix fabric ($w_f > w_p$), the growth of $\sigma_d$ contributed to a decline of $M_r$ of soil mixture, while for the fine aggregate fabric ($w_f < w_p$), the growth of $\sigma_d$ gave rise to an increment of $M_r$.

(2) The $M_r$-$\sigma_d$ relationship for the two fabrics was determined by the competing result between the soil hardening upon loading and the soil rebounding upon unloading. For the fine matrix fabric ($w_f > w_p$), with respect to its high deformability, the rebounding influence on $M_r$ outweighed the hardening influence. Conversely, for the fine aggregate fabric ($w_f < w_p$), the rebounding effect on $M_r$ was secondary compared with the hardening effect based on the consideration of its low deformability.

(3) The combined influences of $w_f$ and $f_v$ on $M_r$ were linked with the influence of suction. Under saturation, the increase of $M_r$ with increasing $f_v$ was explained by the reinforcement influence of coarse grains. Under unsaturation, when the reinforcement influence of incrementing $f_v$ was less significant than the negative influence of decreasing $\psi$, the $M_r$ decreased.


## Acknowledgments

This work is supported by the Jiangxi Provincial Natural Science Foundation of China (Nos. 20224BAB214063, 20224BAB214064, and 20232BAB204083), the National Natural Science Foundation of China (Nos. 52208347 and 52208348), the China Postdoctoral Science Foundation (No. 2023M731436), and the Key Projects of Jiangxi Provincial Department of Water Resources (No. 202426ZDKT01).


## Author contributions

Junyi DUAN designed the research. Yue ZHANG processed the corresponding data. Yu SU wrote the first draft of the manuscript. Jianglin GAO and Zhongzheng WANG helped to organize the manuscript. Da LIU, Bo HAN, and Wenzhe ZHU revised and edited the final version.

## Conflict of interest

Yu SU, Yue ZHANG, Junyi DUAN, Jianglin GAO, Zhongzheng WANG, Da LIU, Bo HAN, and Wenzhe ZHU declare that they have no conflict of interest.

## References


Ahmed S, Lovell Jr CW, Diamond S, 1974. Pore sizes and strength of compacted clay. *Journal of the Geotechnical Engineering Division*, 100(4):407-425. https://doi.org/10.1061/AJGEB6.0000035

Alamanis N, Lokkas P, Chrysanidis T, et al., 2021. Assessment principles for the mechanical behavior of clay soils. *WSEAS Transactions on Applied and Theoretical Mechanics*, 16:47-61. https://doi.org/10.37394/232011.2021.16.6

Anagnostopoulos CA, Chrysanidis T, Anagnostopoulou M, 2020. Experimental data of cement grouting in coarse soils with different superplasticisers. *Data in Brief*, 30:105612. https://doi.org/10.1016/j.dib.2020.105612

ASTM (American Society for Testing and Materials), 2011. Method for Consolidated Drained Triaxial Compression Test for Soils, ASTM D7181-11. ASTM, USA. https://doi.org/10.1520/D7181-11

Bian XC, Wan ZB, Zhao C, et al., 2023. Mud pumping in the roadbed of ballastless high-speed railway. *Géotechnique*, 73(7):614-628. https://doi.org/10.1680/jgeot.21.00135

Cui YJ, Delage P, 1996. Yielding and plastic behaviour of an

unsaturated compacted silt. *Géotechnique*, 46(2):291-311. https://doi.org/10.1680/geot.1996.46.2.291

Delage P, Audiguier M, Cui YJ, et al., 1996. Microstructure of a compacted silt. *Canadian Geotechnical Journal*, 33(1): 150-158. https://doi.org/10.1139/t96-030

Delage P, Marcial D, Cui YJ, et al., 2006. Ageing effects in a compacted bentonite: a microstructure approach. *Géotechnique*, 56(5):291-304. https://doi.org/10.1680/geot.2006.56.5.291

Duong TV, Tang AM, Cui YJ, et al., 2013. Effects of fines and water contents on the mechanical behavior of interlayer soil in ancient railway sub-structure. *Soils and Foundations*, 53(6):868-878. https://doi.org/10.1016/j.sandf.2013.10.006

Duong TV, Cui YJ, Tang AM, et al., 2014. Effect of fine particles on the hydraulic behavior of interlayer soil in railway substructure. *Canadian Geotechnical Journal*, 51(7): 735-746. https://doi.org/10.1139/cgj-2013-0170

Duong TV, Cui YJ, Tang AM, et al., 2016. Effects of water and fines contents on the resilient modulus of the interlayer soil of railway substructure. *Acta Geotechnica*, 11(1): 51-59. https://doi.org/10.1007/s11440-014-0341-0

Gidel G, Hornych P, Chauvin JJ, et al., 2001. A new approach for investigating the permanent deformation behavior of unbound granular material using the repeated load triaxial apparatus. *Bulletin des Laboratoires des Ponts et Chaussées*, 233:5-21.

Hu J, Bian XC, 2022. Analysis of dynamic stresses in ballasted railway track due to train passages at high speeds. *Journal of Zhejiang University-SCIENCE A (Applied Physics & Engineering)*, 23(6):443-457. https://doi.org/10.1631/jzus.A2100305

Indraratna B, Ngo T, Ferreira FB, et al., 2021. Large-scale testing facility for heavy haul track. *Transportation Geotechnics*, 28:100517. https://doi.org/10.1016/j.trgeo.2021.100517

Lamas-López F, 2016. Field and Laboratory Investigation on the Dynamic Behaviour of Conventional Railway Track-Bed Materials in the Context of Traffic Upgrade. PhD Thesis, Université Paris-Est, Paris, France.

Lekarp F, Isacsson U, Dawson A, 2000. State of the art. I: resilient response of unbound aggregates. *Journal of Transportation Engineering*, 126(1):66-75. https://doi.org/10.1061/(ASCE)0733-947X(2000)126:1(66)

Li X, Zhang LM, 2009. Characterization of dual-structure pore-size distribution of soil. *Canadian Geotechnical Journal*, 46(2):129-141. https://doi.org/10.1139/T08-110

Lokkas P, Chouliaras I, Chrisanidis T, et al., 2021. Historical background and evolution of soil mechanics. *WSEAS Transactions on Advances in Engineering Education*, 18:96-113. https://doi.org/10.37394/232010.2021.18.10

Muñoz-Castelblanco JA, Pereira JM, Delage P, et al., 2012. The water retention properties of a natural unsaturated loess from northern France. *Géotechnique*, 62(2):95-106. https://doi.org/10.1680/geot.9.P.084

Ng CWW, Zhou C, Yuan Q, et al., 2013. Resilient modulus of unsaturated subgrade soil: experimental and theoretical investigations. *Canadian Geotechnical Journal*, 50(2):223-232. https://doi.org/10.1139/cgj-2012-0052

Ng CWW, Baghbanrezvan S, Sadeghi H, et al., 2017. Effect of specimen preparation techniques on dynamic properties of unsaturated fine-grained soil at high suctions. *Canadian Geotechnical Journal*, 54(9):1310-1319. https://doi.org/10.1139/cgj-2016-0531

Ng CWW, Lu BW, Ni JJ, et al., 2019. Effects of vegetation type on water infiltration in a three-layer cover system using recycled concrete. *Journal of Zhejiang University-SCIENCE A (Applied Physics & Engineering)*, 20(1):1-9. https://doi.org/10.1631/jzus.A1800373

Qi S, Cui YJ, Chen RP, et al., 2020a. Influence of grain size distribution of inclusions on the mechanical behaviours of track-bed materials. *Géotechnique*, 70(3):238-247. https://doi.org/10.1680/jgeot.18.P.047

Qi S, Cui YJ, Dupla JC, et al., 2020b. Investigation of the parallel gradation method based on the response of track-bed materials under cyclic loadings. *Transportation Geotechnics*, 24:100360. https://doi.org/10.1016/j.trgeo.2020.100360

Su Y, Cui YJ, Dupla JC, et al., 2020. Investigation of the effect of water content on the mechanical behavior of track-bed materials under various coarse grain contents. *Construction and Building Materials*, 263:120206. https://doi.org/10.1016/j.conbuildmat.2020.120206

Su Y, Cui YJ, Dupla JC, et al., 2021a. Developing a sample preparation approach to study the mechanical behavior of unsaturated fine/coarse soil mixture. *Geotechnical Testing Journal*, 44(4):20190450. https://doi.org/10.1520/GTJ20190450

Su Y, Cui YJ, Dupla JC, et al., 2021b. Effect of water content on resilient modulus and damping ratio of fine/coarse soil mixtures with varying coarse grain contents. *Transportation Geotechnics*, 26:100452. https://doi.org/10.1016/j.trgeo.2020.100452

Su Y, Cui YJ, Dupla JC, et al., 2022. Soil-water retention behaviour of fine/coarse soil mixture with varying coarse grain contents and fine soil dry densities. *Canadian Geotechnical Journal*, 59(2):291-299. https://doi.org/10.1139/cgj-2021-0054

Sun QD, Indraratna B, Nimbalkar S, 2016. Deformation and degradation mechanisms of railway ballast under high frequency cyclic loading. *Journal of Geotechnical and Geoenvironmental Engineering*, 142(1):04015056. https://doi.org/10.1061/(ASCE)GT.1943-5606.0001375

Sun Y, Nimbalkar S, Chen C, 2018. Grading and frequency dependence of the resilient modulus of ballast. *Géotechnique Letters*, 8(4):305-309. https://doi.org/10.1680/jgele.18.00084

Trinh VN, 2011. Comportement Hydromécanique de Matériaux Constitutifs de Plateformes Ferroviaires Anciennes. PhD Thesis, Université Paris-Est, Paris, France (in French).

Trinh VN, Tang AM, Cui YJ, et al., 2012. Mechanical characterisation of the fouled ballast in ancient railway track

substructure by large-scale triaxial tests. *Soils and Foundations*, 52(3):511-523. https://doi.org/10.1016/j.sandf.2012.05.009

Wan ZB, Bian XC, Li SH, et al., 2020. Remediation of mud pumping in ballastless high-speed railway using polyurethane chemical injection. *Construction and Building Materials*, 259:120401. https://doi.org/10.1016/j.conbuildmat.2020.120401

Wang HL, Cui YJ, Lamas-Lopez F, et al., 2017. Effects of inclusion contents on resilient modulus and damping ratio of unsaturated track-bed materials. *Canadian Geotechnical Journal*, 54(12):1672-1681. https://doi.org/10.1139/cgj-2016-0673

Wang HL, Cui YJ, Lamas-Lopez F, et al., 2018a. Investigation on the mechanical behavior of track-bed materials at various contents of coarse grains. *Construction and Building Materials*, 164:228-237. https://doi.org/10.1016/j.conbuildmat.2017.12.209

Wang HL, Cui YJ, Lamas-Lopez F, et al., 2018b. Permanent deformation of track-bed materials at various inclusion contents under large number of loading cycles. *Journal of Geotechnical and Geoenvironmental Engineering*, 144(8):04018044. https://doi.org/10.1061/(ASCE)GT.1943-5606.0001911

Wang HL, Chen RP, Cheng W, et al., 2019. Full-scale model study on variations of soil stress in geosynthetic-reinforced pile-supported track bed with water level change and cyclic loading. *Canadian Geotechnical Journal*, 56(1):60-68. https://doi.org/10.1139/cgj-2017-0689

Werkmeister S, Dawson AR, Wellner F, 2001. Permanent deformation behavior of granular materials and the shakedown concept. *Transportation Research Record: Journal of the Transportation Research Board*, 1757(1):75-81. https://doi.org/10.3141/1757-09

Werkmeister S, Dawson AR, Wellner F, 2004. Pavement design model for unbound granular materials. *Journal of Transportation Engineering*, 130(5):665-674. https://doi.org/10.1061/(ASCE)0733-947X(2004)130:5(665)

Yang SR, Lin HD, Kung JHS, et al., 2008. Suction-controlled laboratory test on resilient modulus of unsaturated compacted subgrade soils. *Journal of Geotechnical and Geoenvironmental Engineering*, 134(9):1375-1384. https://doi.org/10.1061/(ASCE)1090-0241(2008)134:9(1375)

Zhang F, Cui YJ, Zeng LL, et al., 2018. Effect of degree of saturation on the unconfined compressive strength of natural stiff clays with consideration of air entry value. *Engineering Geology*, 237:140-148. https://doi.org/10.1016/j.enggeo.2018.02.013

Zheng H, Zhang C, Yang Z, 2020. A local radial basis function collocation method for band structure computation of 3D phononic crystals. *Applied Mathematical Modelling*, 77:1954-1964. https://doi.org/10.1016/j.apm.2019.09.006

## Electronic supplementary materials

Sections S1 and S2